Investigation of Collimator Influential Parameter on SPECT Image Quality: a Monte Carlo Study

Banari Bahnamiri Sh.[1]*

[1]Assistant Professor of Nuclear Physics, Tabari University of Babol, Iran

ABSTRACT

Background: Obtaining high quality images in Single Photon Emission Tomography (SPECT) device is the most important goal in nuclear medicine. Because if image quality is low, the possibility of making a mistake in diagnosing and treating the patient will rise. Studying effective factors in spatial resolution of imaging systems is thus deemed to be vital. One of the most important factors in SPECT imaging in nuclear medicine is the use of an appropriate collimator for a certain radiopharmaceutical feature in order to create the best image as it can be effective in the quantity of Full Width at Half Maximum (FWHM) which is the main parameter in spatial resolution.

Method: In this research, the simulation of the detector and collimator of SPECT imaging device, Model HD3 made by Philips Co. and the investigation of important factors on the collimator were carried out using MCNP-4c code.

Results: The results of the experimental measurments and simulation calculations revealed a relative difference of less than 5% leading to the confirmation of the accuracy of conducted simulation MCNP code calculation.

Conclusion: This is the first essential step in the design and modelling of new collimators used for creating high quality images in nuclear medicine.

Keywords

Collimator, FWHM, MCNP-4C, SPECT, Monte Carlo simulation

Introduction

The study of the inside of the body to diagnose a disease without surgical methods is done through imaging in nuclear medicine. Single-Photon Emission Computed Tomography (SPECT), a type in which gamma photon–emitting radionuclides are administered and then detected by one or more gamma cameras rotated around the patient, using series of two-dimensional images to recreate a three-dimensional view. A lot of studies are focused on obtaining high-resolution images [1-8]. Also, Several studies on the spatial resolution of SPECT have shown that resolution varies with source–detector distance and the collimator [13-22] because a correct diagnosis using a high quality image can help physicians to provide effective treatment. Hence, it is necessary to examine factors affecting the quality of the images created by imaging devices. One of the most important factors in imaging in nuclear medicine is the use of an appropriate collimator for a certain radiopharmaceutical in order to create the best image because it can be effective on the quantity

*Corresponding author: Sh. Banari Bahnamiri Assistant Professor of Nuclear Physics, Tabari University of Babol, Sardaran 9, Sheykh TABARSI St., Babol, Iran
E-mail: banari92@gmail.com

of Full Width at Half Maximum (FWHM) which is the main parameter in measuring image clarity [9]. Indeed, Spatial resolution quantifies the size of the smallest object that can be resolved reliably, and is often expressed as the FWHM of a point spread function. For projection data acquired with an gamma camera, the total resolution depends on the intrinsic resolution and the collimator resolution [10] as in figure 1.

SPECT image reconstruction requires that the incident direction of each acquired count be known. An external collimator is used to do so. Therefore, the design of collimators for creating the image of each radionuclide, especially for new radionuclide such as synthetic radiopharmaceutical, is very important. In this research, this was in an effort to obtain a reasonable method for designing parallel collimator. So, we simulated Hexagona collimator and detector of the SPECT system and investigated the most important parameters affecting FWHM.

Material And Methods

The majority of SPECT systems are based on gamma camera technology where one or more cameras rotate about the body of the patient. A gamma camera consists of a single crystal NaI (Tl), which absorbs incident gamma photons and scintillates or emits light in response, in back of which there are banks of photomultiplier tubes (PMTs) and electronics to compute gamma ray energy and the location of scintillation within crystal. The structure of a parallel-hole collimator [11] is similar to that of a honeycomb consisting of a large number of hexagonal narrow channels separated by thin septa whose length, diameter, wall thickness and forming material can play an important role in the clarity of images because the beams which directly reach the hole from the organ are only allowed to pass by the collimator, and other beams emitted from any other side are eliminated. However, there are virtually some problems leading to a lower image quality. The first problem is that the sensitivity of the device decreases by the collimator i.e. fewer photons reach NaI (Tl) crystal and produce light. The second problem is that there may still be other beams which

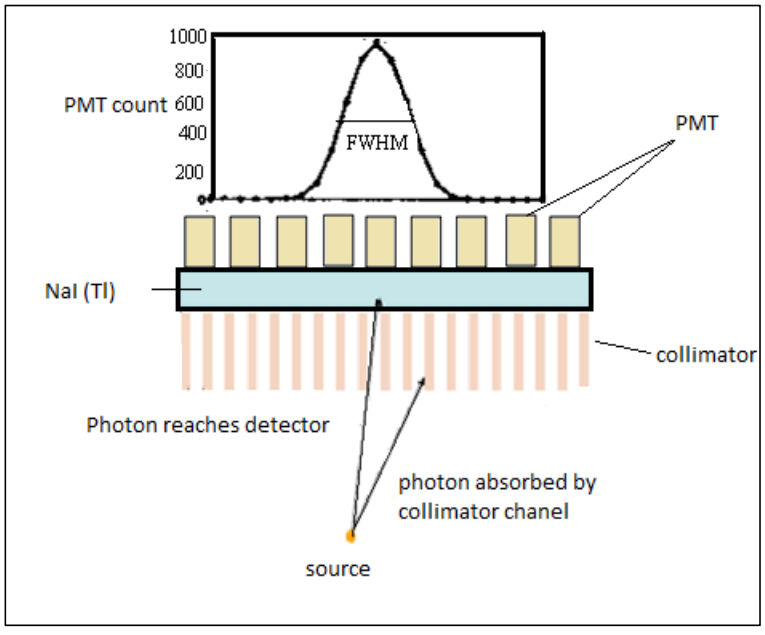

Figure 1: Cross-Sectional View of a SPECT System

directly enter collimator's holes due to dispersal from other areas of the body, except the one under the hole, and produce light in NaI (Tl) crystal causing a reduction in image quality. The third potential problem concerns the fact that some photons may not be prevented in collimator wall and may pass it in some cases. The role of these beams in image quality is known as "wall effect". For instance, this effect for a point source causes a considerable count of gamma in its first six neighboring holes as well as multiplier tube just under the hole above the source; consequently, seven bright star-shaped points will be observed instead of a single one.

Simulation of SPECT Detector Section

The simulated detection of SPECT system consists of a hexagonal collimator, NaI (Tl) crystal and PMTs. The dimensions of different parts of SPECT system (HD31, Philips Manufacturer) in this work are as follows: NaI (Tl) crystal (0.95cm × 59.1cm × 44.5cm) and under crystal/PMT array, a hexagonal collimator (59.1cm × 44.5cm × 5.08 cm) on which there are about 8000 holes (Diameter = 3.4mm, height = 5.08cm and thickness is 2mm). There are 65 PMT tubes in contact with the crystal in an hexagonal arrangement. Both collimator and crystal are surrounded by a shield made of lead. The dimensions of the front and back shields are (1.27cm × 6.98cm × 59.1cm), those of the left and right ones are (44.5cm × 6.98cm × 59.1cm) and that of the top one is 44.5cm × 59.1cm × 0.95cm. The cards used in this simulation were LAT, U, FILL, TRCL, MN, F8 and DBCN card [12].

Examination of detector response function based on Gaussian distribution was necessary in this simulation. Knowing detector response function in involved energies was required to consider the energy window for the elimination of the dispersed beams. Depending on its forming materials and composition as well as its physical and geometric characteristics in different energies, each detector has different separation efficiency and response functions. The data related to the detector's separation ability is not included in MCNP code, and the characteristics of the experimental spectrum should be defined for the code whenever detector's experimental spectrum is important in calculations. The detector's experimental spectrum NaI (Tl) was measured for energies 140KeV and 511keV, and the response function applied in the simulation was obtained using experimental spectrum.

An Examination of Experimental and Simulation Results for Code Assessment

After simulating different parts of SPECT's detection device, a point source was defined in the code in front of the hexagonal collimator and 10cm apart, and the value of FWHM in the energy 140keV (TC-99m) was calculated. The result was compared to the characteristics of the device announced by producer factory. Then, the value of FWHM was measured for TC-99m source with energy of 140keV experimentally. TC-99m was placed in a cylindrical container with a length of 5cm and a diameter of 1.66cm.

Continuing code assessment with experimental results, different values of FWHM for different distances from the source (140 keV) to the collimator were examined. Both linear and point sources in computational method, and the linear source in experimental one were placed at distances of 100 mm, 120 mm, 140 mm, 160 mm, 180 mm and 200 mm. Results are shown in figure 2. Moreover, the values of FWHM for different distances from the source 511 keV to the collimator were examined by the code. In computational method, both linear and point

sources were placed at distances of 100 mm, 120 mm, 140 mm, 160 mm, 180 mm and 200 mm. The results are indicated in figure 3 along with identical values for the source 140 keV.

Experimental and Computational Measurement of FWHM from Dispersing Environment

In order to study the effect of dispersing environment on FWHM value, the distance between the source and the collimator was considered to be 20 cm, and different thicknesses of polyethylene (dispersing environment) were placed between the collimator and the source. Results of calculating and measuring value of FWHM for linear and point sources in each thickness are illustrated in figure 4.

Examination of Penetration Effect through Wall (Wall Effect) for Sources 140 keV and 511 keV

The linear source 140 keV was placed 1

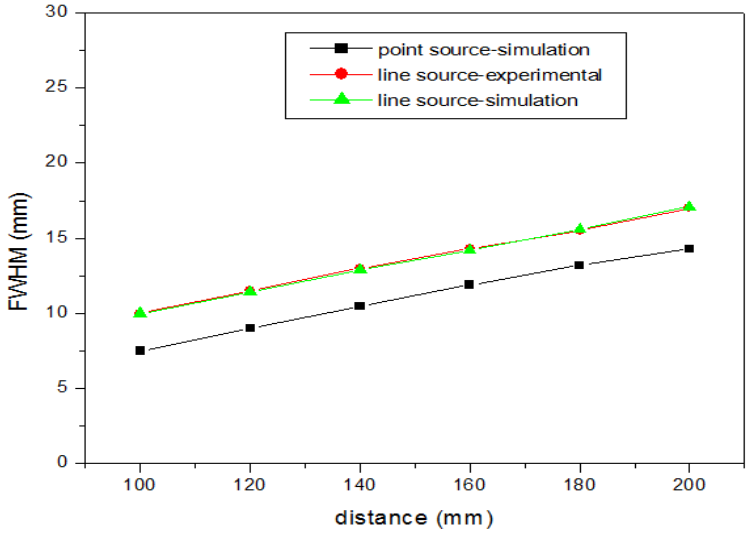

Figure 2: Different Values of FWHM based on Distance from the Source 140 keV to Collimato

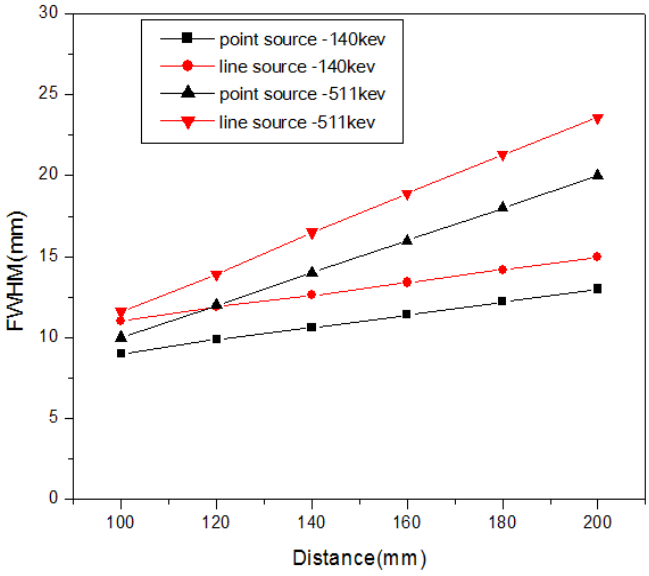

Figure 3: Different Values of FWHM according to Distance from 140 keV and 511 keV Sources to Collimator

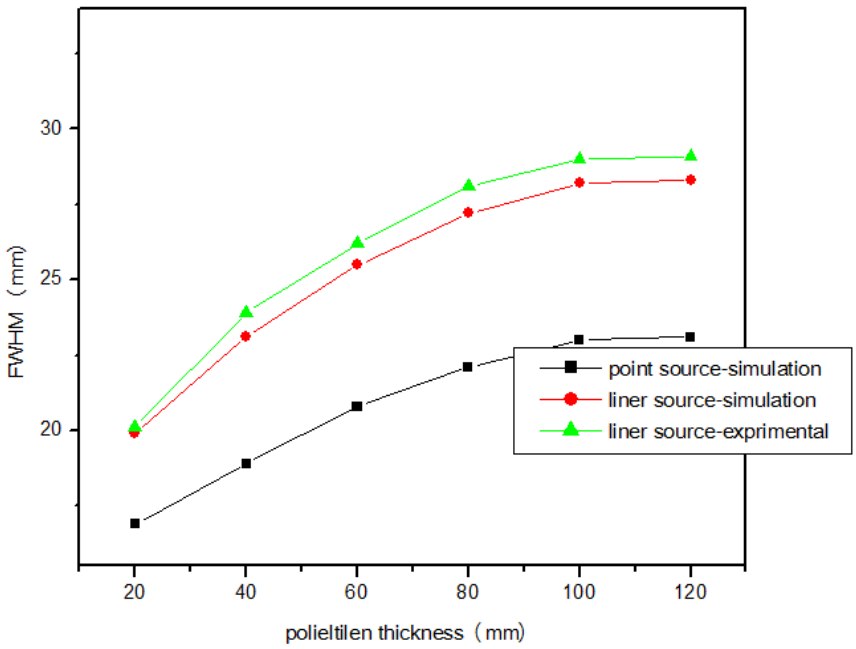

Figure 4: Different Values of FWHM according to Polyethylene Thickness when the Source 140 keV is Located 20 cm apart from Collimator

mm away from collimator in order to measure this effect experimentally. Then, gamma count was registered in multiplier tubes of the central ax and the first and second neighbors. Central ax is actually a row of collimator holes and multiplier tubes placed right above the linear source; the first and second neighbors include the first and second rows on the right and left of the central ax. This process was carried out for five rows located vertically next to the central ax. The first row is just next to the middle point of the source (middle row) and the next four rows are the first to the fourth neighbors of the middle row. Same procedure was also followed to examine the source 511 keV; however, an appropriate linear source was not available. Therefore, the resulted count was produced by simulation.

Results and Discussion

Studying experimental and simulation results for code assessment is illustrated in table 1. As it can be seen in the table, values of FWHM in the simulation and the report of the Philips Company are 8.8 mm and 8.8±0.8 mm, respectively revealing appropriate agreement. However, final experimental value of FWHM is 10.8 mm. The main difference which was noticed arises from the fact that the system was not in its ideal conditions including such problems as the existing non-point source and a device which was not calibrated. The value of FWHM for a calibrated SPECT system was found to be 10.21 mm. Its difference with the value of 8.8 mm concerns non-point source. To make sure of this issue, the linear Tc-99m source was simulated instead of the point source and the result of the new calculation of FWHM was 10.17 mm having a relative difference of 4% with experimental value of (=10.21 mm) and thus being acceptable. All succeeding measurements were taken after calibrating the device. Moreover, it can be seen in figures 5 and 6 that the part related to the peak of simulated response function shows Gaussian fit on experimental spectrum; this agreement is obvious in the curve. The measurement and calculation of the val-

Table 1: Results of Experiment and Simulat

Conditions of the Source and the Revealer	FWHM (mm)
Features reported by the manufacturer	8.8±0.8
Calculation with the point source	8.8
Measurement without calibration (the linear source)	8. 10
Measurement after calibration (the linear source)	21. 10
Calculation with the linear source	17 . 10

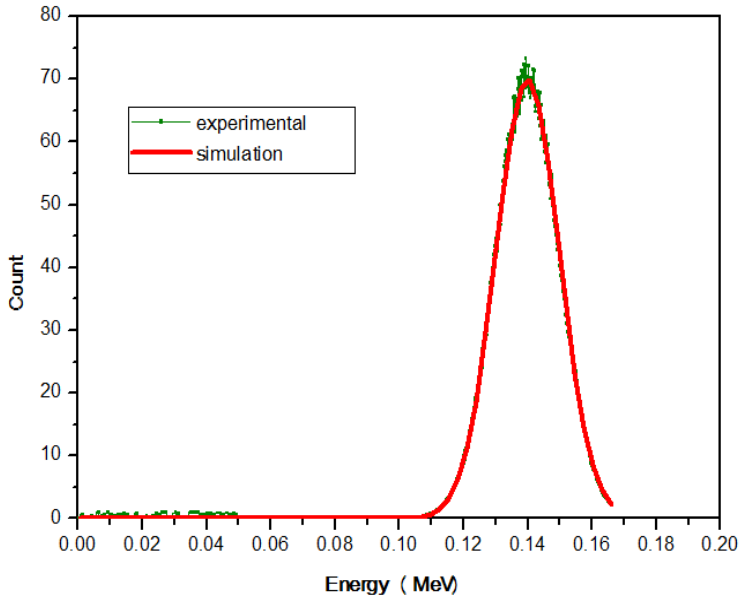

Figure 5: Experimental Detector Spectrum NaI (Tl) and its Simulated Response Function for the Energy 140 KeV

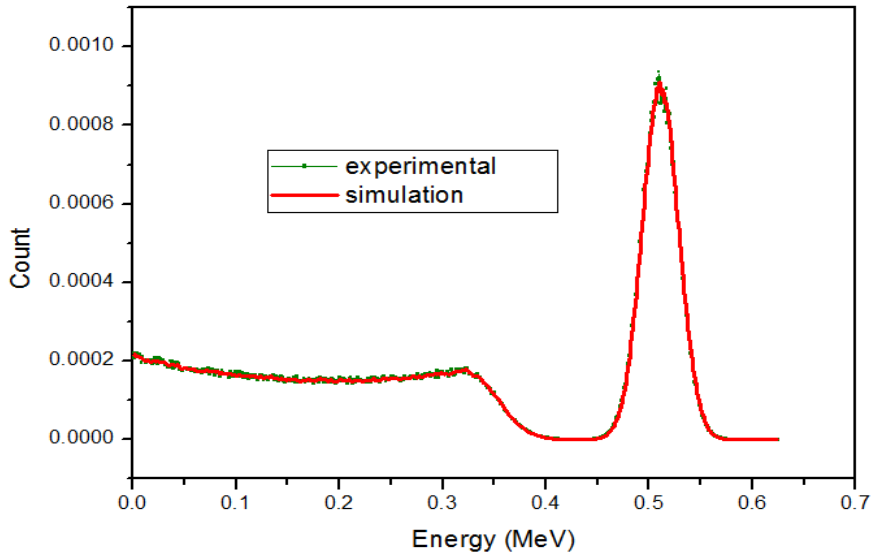

Figure 6: Experimental Revealer Spectrum NaI (Tl) and its Simulated Response Function for the Energy 511 KeV

ues of FWHM for the source 140 keV are illustrated in figure 2. The results of the simulation of the point source contain a statistical error of about 2.15%. Concerning linear source, the agreement between experimental and simulation results is clear and statistical errors of simulation and experimental results are 2% and 3%, respectively. In spite of the difference in the values resulted from linear and point sources, the curves indicate almost similar slopes. The slopes of the fitted line on computational point, linear sources and experimental linear source were 0.058, 0.065 and 0.066, respectively. On the average, the growth of FWHM in relation to distance from the source to the collimator is 10.9%, 10.8% and 10.7% for the point source, the linear source of the computational method and the experimental source, respectively.

Results of simulation calculations for both sources are shown in figure 3. It can be found from the curve that the value of FWHM increases with the rise in energy as well as the conversion of the point source into the linear one. Experimental and computational measurement of FWHM resulting from dispersing environment can be seen in figure 4. As one can see, values of FWHM have surged in this figure.

The results of examining penetration effect through the wall for the sources of 140 keV and 511 keV are displayed in figures 7 and 8. If penetration from the wall had not taken place, the counted number for all multiplier tubes would have been zero except for the central ax. However, as it can be noticed in figure 8, the count of photomultiplier tubes of the first neighbor is considerable. The lower the role of the penetration of the collimator wall, the more appropriate the image quality will be. It can be viewed in figure 8 that the count in photomultiplier tubes of the central ax has fallen in comparison to the source 140 keV while the count of the photomultiplier tubes of the first neighbor in some rows has increased up to about 45% of the count of the central ax. Also, the count of the photomultiplier tubes of the second neighbor is significant.

As it is shown in figure 2, the value of

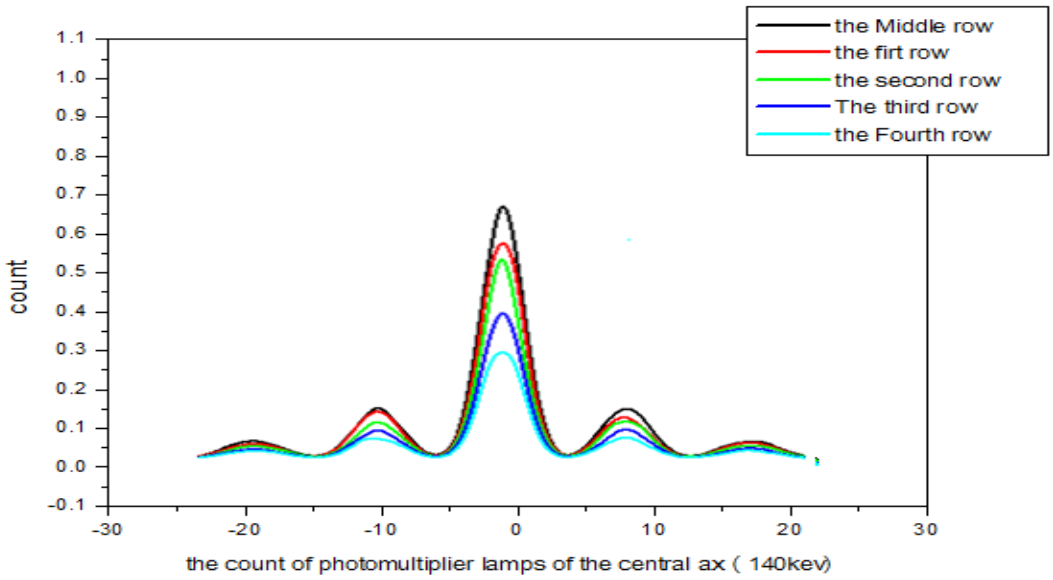

Figure 7: Counts of Photomultiplier Lamps of Central Ax and the First and Second Neighbors. Five Graphs are Drawn for Five Different Rows. Energy of the Source is 140 keV.

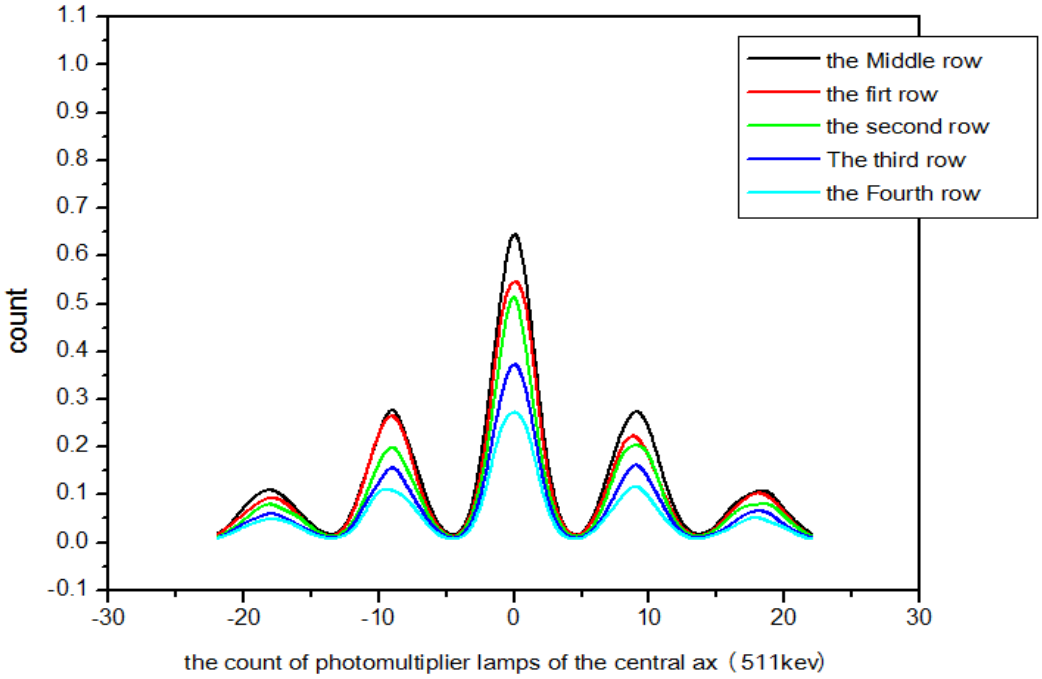

Figure 8: Counts of Photomultiplier Lamps of Central Ax and the First and Second Neighbors. Five Graphs are Drawn for Five Different Rows. Energy of the Source is 511 keV.

FWHM goes up by the conversion of the point source into the linear one. The main cause of this increase is the distribution of the source in thickness with a diameter of 1.66 mm in Tc-99m cylinder. The value of FWHM also rises in figure 3 with the increase in energy that is principally due to gamma penetrating the wall. In figure 4, the width of FWHM surges with the rise in polyethylene thickness as the dispersing environment. This width increase occurs firstly due to the presence of dispersing environment which causes photons to disperse all over the collimator surface, and secondly because it is highly probable for the energy of this gamma to disperse in polyethylene environment and then reach collimator, and the energy of this gamma may also lie in the energy window range. So, there is also gamma count in the photomultiplier tubes which are not related to the collimators above the source. The width of FWHM thus rises.

Simulated collimator is applied to take photos of cardiovascular organs of the body using involved radiopharmaceutical (Tc-99m). Calculations and experiments in figure 2 have shown that the growth rates of FWHM per distance are about 10.7% and 10.9% for this source. Therefore, a distance of 10 cm is normally chosen for imaging. Adding dispersing environment between the source and the collimator approximately increases FWHM for 10% while this effect can be removed to a great extent by narrowing the energy window. As it can be seen in figure 7, the wall effect is ignorable except in the first neighbor. A fraction of penetrated photons have the energy out of the energy window and will be omitted. However, the photon which goes through the wall whose energy lies in the energy window span will be counted. In order to remove this effect, the number of photons penetrating into the wall should be calculated for each set of conditions and then subtracted from the photomultiplier tubes count. Regarding this description, this collimator almost meets the conditions required for receiving an ap-

propriate image from the photon source 140 keV.

In addition, in order to test the effect of this collimator in imaging from gamma sources resulting from paired destruction (511 keV), one can see that the value of FWHM e(figure 3) as well as the penetration into the wall (figure 8) have increased with the increase in the energy from 140 keV to 511 keV. The possibility of Compton dispersal in interaction with environment rises with increased photon energy. If the photon emitted from the source 511 keV reaches detector after dispersal, it may be regarded in the photoelectric peak count and thus leads to defects in image. The energy window should be made smaller to omit such beams leading to lower efficiency. If emitted photon reaches the detector after two or three dispersals and if its energy does not lie in the energy window range, it will be omitted. Dispersal increase, however, brings about lower efficiency. On the other hand, the increase in photon energy makes trapping in walls difficult. Either the thickness of the walls has definitely got to be raised or the material of the collimator should change in a way to minimize penetration into the wall in order to have a good image from the source 511 keV. Having applied the energy window, calculated values of FWHM for the energy 511 keV was averagely 24% higher than identical values in the energy 140 keV that will definitely not lead to good results. For these reasons, using hexagonal collimators for the energy 140 keV in providing images from 511 keV sources is not recommended.

Conclusion

The main purpose of this study was to devise a suitable method for designing new collimators. In this research, we simulated an hexagonal collimator and the detector of SPECT device. Results of the study reveal that there is good agreement between simulation calculations and experimental measurements with a difference of less than 5% which even gets more acceptable after calibrating the system and using a linear source. Indeed, the agreement between simulation and experimental measurements and the investigations of effective parameters of the collimator is the first essential step in achieving this goal. So, one can model a new collimator for new/compound radiopharmaceutical that may be made in the future by changing the parameters in the simulation process.

Acknowledgment

This work was supported by Ferdowsi University of Mashhad, Imam Reza Hospital and Tabari University of Babol.

Conflict of Interest

None

References

1. Rosenthal MS, Cullom J, Hawkins W, Moore SC, Tsui BM, Yester M. Quantitative SPECT imaging: a review and recommendations by the Focus Committee of the Society of Nuclear Medicine Computer and Instrumentation Council. *J Nucl Med*. 1995;**36**(8):1489-513. PubMed PMID: 7629599.
2. Devous MD Sr, Thisted RA, Morgan GF, Leroy RF, Rowe CC. SPECT brain imaging in epilepsy: a meta-analysis. *J Nucl Med*. 1998;**39**(2):285-93. PubMed PMID: 9476937.
3. James ML, Gambhir SS. A molecular imaging primer: modalities, imaging agents, and applications. *Physiol Rev*. 2012;**92**(2):897-965. doi: 10.1152/physrev.00049.2010. PubMed PMID: 22535898.
4. Weber DA, Ivanovic M, Franceschi D, Strand SE, Erlandsson K, Franceschi M, et al. Pinhole SPECT: an approach to in vivo high resolution SPECT imaging in small laboratory animals. *J Nucl Med*. 1994;**35**(2):342-8. PubMed PMID: 8295008.
5. Takahashi Y, Murase K, Mochizuki T, Higashino H, Sugawara Y, Kinda A. Evaluation of the number of SPECT projections in the ordered subsets-expectation maximization image reconstruction method. *Ann Nucl Med*. 2003;**17**(7):525-30. PubMed PMID: 14651350.

6. Takahashi Y, Murase K, Mochizuki T, Higashino H, Sugawara Y, Kinda A. Segmented attenuation correction for myocardial SPECT. *Ann Nucl Med*. 2004;**18**(2):137-43. PubMed PMID: 15195761.
7. Takahashi Y, Miyagawa M, Nishiyama Y, Ishimura H, Mochizuki T. Performance of a semiconductor SPECT system: comparison with a conventional Anger-type SPECT instrument. *Ann Nucl Med.* 2013;**27**(1):11-6. doi: 10.1007/s12149-012-0653-9. PubMed PMID: 22956363; PubMed Central PMCID: PMC3549244.
8. Chun SY, Fessler JA, Dewaraja YK. Correction for collimator-detector response in SPECT using point spread function template. *IEEE Trans Med Imaging*. 2013;**32**(2):295-305. doi: 10.1109/tmi.2012.2225441. PubMed PMID: 23086521; PubMed Central PMCID: PMC3619230.
9. Takahashi Y, Murase K, Mochizuki T, Sugawara Y, Maeda H, Kinda A. Simultaneous 3-dimensional resolution correction in SPECT reconstruction with an ordered-subsets expectation maximization algorithm. *J Nucl Med Technol*. 2007;**35**(1):34-8. PubMed PMID: 17337655.
10. Jaszczak RJ, Li J, Wang H, Zalutsky MR, Coleman RE. Pinhole collimation for ultra-high-resolution, small-field-of-view SPECT. *Phys Med Biol*. 1994;**39**(3):425-37. PubMed PMID: 15551591.
11. Seo Y, Wong KH, Sun M, Franc BL, Hawkins RA, Hasegawa BH. Correction of photon attenuation and collimator response for a body-contouring SPECT/CT imaging system. *J Nucl Med*. 2005;**46**(5):868-77. PubMed PMID: 15872362.
12. Briesmeister JF. MCNP: A General Monte Carlo N-Particle Transport Code, Version 4C. Los Alamos: Los Alamos National Laboratory; 2000 April. Report No: LA-13709-M.
13. Edholm PR, Lewitt RM, Lindholm B. Novel properties of the Fourier decomposition of the sonogram. In: Budinger TF, Cho ZH, Nalcioglu O, editors. Proceedings SPIE 0671, Physics and Engineering of Computerized Multidimensional Imaging and Processing; 1986 Jan 1; Newport Beach, California: SPIE,The International Society for Optical Engineering; 1986. p 8-18. doi:10.1117/12.966672.
14. Maniawski PJ, Morgan HT, Wackers FJ. Orbit-related variation in spatial resolution as a source of artifactual defects in thallium-201 SPECT. *J Nucl Med*. 1991;**32**(5):871-5. PubMed PMID: 2022998.
15. Zeng GL, Gullberg GT. Frequency domain implementation of the three-dimensional geometric point response correction in SPECT imaging. *IEEE Trans Nucl Sci*. 1992;**39**:1444-53. doi: 10.1109/23.173222.
16. Tsui BMW, Zhao X, Frey EC, Gullberg GT. Comparison between ML-EM and WLS-CG algorithms for SPECT image reconstruction. *IEEE Trans Nucl Sci*. 1991;**38**:1766-72. doi: 10.1109/23.124174.
17. Glick SJ, Penney BC, King MA, Byrne CL. Noniterative compensation for the distance-dependent detector response and photon attenuation in SPECT imaging. *IEEE Trans Med Imaging*. 1994;**13**(2):363-74. doi: 10.1109/42.293929. PubMed PMID: 18218512.
18. Hutton BF, Lau YH. Application of distance-dependent resolution compensation and post-reconstruction filtering for myocardial SPECT. *Phys Med Biol*. 1998;**43**(6):1679-93. PubMed PMID: 9651033.
19. Kohli V, King MA, Glick SJ, Pan TS. Comparison of frequency-distance relationship and Gaussian-diffusion-based methods of compensation for distance-dependent spatial resolution in SPECT imaging. *Phys Med Biol*. 1998;**43**(4):1025-37. PubMed PMID: 9572525.
20. Shinohara H, Yamamoto T, Sugimoto H, Hashimoto T, Takahashi M, Yokoi T. [Scatter, attenuation and detector response correction of SPECT]. *Med Image Technol.* 2000;**18**:24-32. (Jpn).
21. Yokoi T, Shinohara H, Onishi H. Performance evaluation of OSEM reconstruction algorithm incorporating three-dimensional distance-dependent resolution compensation for brain SPECT: a simulation study. *Ann Nucl Med.* 2002;**16**(1):11-8. PubMed PMID: 11922203.
22. Maeda H, Yamaki N, Natsume T, Takeda K, Hasebe S, Kinda A, et al. [Simultaneous spatial resolution correction in SPECT reconstruction using OS-EM algorithm]. *Igaku Butsuri*. 2004;**24**(2):61-71. PubMed PMID: 15383710. (Jpn).